




# Carbon nanofibers addition on transport and superconducting properties of bulk $\text{YBa}_2\text{Cu}_3\text{O}_{7-\delta}$ material prepared via co-precipitation

Nurul Auni Khalid<sup>1</sup>, Mohd Mustafa Awang Kechik<sup>1,\*</sup> , Nur Atikah Baharuddin<sup>1</sup>, Chen Soo Kien<sup>1</sup>, Hussein Baqiah<sup>1</sup>, Lim Kean Pah<sup>1</sup>, Abdul Halim Shaari<sup>1</sup>, Zainal Abidin Talib<sup>1</sup>, Azhan Hashim<sup>2</sup>, Masato Murakami<sup>3</sup>, and Muralidhar Miryala<sup>3</sup>

<sup>1</sup>Department of Physics, Faculty of Science, Universiti Putra Malaysia, 43400 UPM Serdang, Selangor, Malaysia

<sup>2</sup>Faculty of Applied Sciences, Universiti Teknologi MARA Pahang, 26400 Jengka, Pahang, Malaysia

<sup>3</sup>Shibaura Institute of Technology, 3 Chome-7-5 Toyosu, Koto, Tokyo 135-8548, Japan

Received: 31 March 2020

Accepted: 12 August 2020

Published online:

5 September 2020

© The Author(s) 2020

## ABSTRACT

The effects of carbon nanofibers addition on transport and superconducting properties of  $\text{YBa}_2\text{Cu}_3\text{O}_{7-\delta}$  (Y-123) superconductor were studied. Y-123 was prepared using co-precipitation method for good quality bulk of high temperature superconducting material. Carbon nanofibers with 0.2–0.8 wt% were added into Y-123 superconductors. The samples were characterized using electrical resistance measurement for critical temperature ( $T_c$ ) and critical current density ( $J_c$ ), powder X-ray diffraction, scanning electron microscopy and energy-dispersive X-ray analysis. Most of the samples indicated a dominant Y-123 phase of an orthorhombic structure with a minor phase of  $\text{BaCO}_3$  and Y-124. Onset critical temperature was found to decrease from 90.5 to 80 K with increasing of carbon nanofibers concentration. The  $J_c$  for pure sample is 11  $\text{A}/\text{cm}^2$  at 30 K while the  $J_c$  of sample with 0.4 wt% carbon nanofibers is 830  $\text{A}/\text{cm}^2$  at 30 K. Introduction of carbon nanofibers enhanced  $J_c$  significantly. However, further addition of carbon nanofibers in Y-123 superconductor caused degradation in  $J_c$ .

## 1 Introduction

A revolutionary discovery of YBCO or Y-123 with chemical formula of  $\text{YBa}_2\text{Cu}_3\text{O}_{7-\delta}$  was the first ever material discovered to show  $T_c$  above the boiling point of liquid nitrogen (77 K) [1, 2]. This simply means that superconductors would no longer require a complex cooling system for their applications unlike other materials that rely on liquid helium for their operation which is rather costly. Due to its high

$T_c$ , Y-123 system may become potential superconducting materials for future applications. The material has been recognized as second generation high temperature superconductors (HTS) and gave huge impacts to the market penetration for technology and power applications [3]. However, the weak flux pinning and granularity of Y-123 especially at temperatures above 20–30 K seems to limit the value of  $J_c$  [4].

Many groups claim that the improvement of  $J_c$  in high temperature superconductor can be obtained by

the introduction of nanoparticle addition. The addition of  $\text{Fe}_3\text{O}_4$ , Zn and Zr nanoparticles acted as effective flux pinning centers in Y-123 superconductor and improved the  $J_c$  [5–7]. Also the improvement of  $J_c$  and suppression of  $T_c$  were observed by the addition of nano-Ag in (Bi,Pb)-2223 superconductor [8]. The effective artificial pinning centers will further enhance  $J_c$  at higher fields [9] and higher temperature. This could be achieved when the flux lines are pinned and their movement are prevented [10]. In high temperature superconductor (HTS), the effects on the vortex movements, determination of  $J_c$ , and other superconducting properties are depend on the engineering artificial pinning centers which pin flux lines through crystal imperfections [11] or so-called defects [12] such as low-angle grain boundaries, twin boundaries, dislocations and non-superconducting phases [13, 14]. The route of artificially introducing inhomogeneity or second-phase materials as flux pinning sites in the processing of bulk YBCO is a long standing issue [15].

Other flux pinning approach can be done by applying high pressure onto superconductors [12]. It has been found that by using 1 GPa hydrostatic pressure, more effective point pinning centers, can be introduced in  $\text{NaFe}_{0.97}\text{Co}_{0.03}\text{As}$  single crystal in comparison with that at 0 GPa [13]. An enhancement of critical current density of  $(\text{Ba,K})\text{Fe}_2\text{As}_2$  single crystals up to fivefold in low and high magnetic field through improvement of flux pinning was obtained by applying 1.2 GPa hydrostatic pressure [14].

A technique of doping and addition of impurities including metal and non-metal elements, nanoparticles, carbon sources and other compounds have shown significant effect on the superconducting properties. Various forms of oxides can be considered for selection of dopant [16–19]. Carbon nanotubes have been widely used as a filler for nanocomposites by the virtue of their structural, electrical, magnetic properties and exhibit a great potential application to enhance current-carrying capability of superconductors and as a wide-band electromagnetic wave absorber [20, 21]. It has been shown that of the choice of the type and amount of chemical compound and impurities could improve both inter-granular and intra-granular  $J_c$  in different high temperature superconductors [4, 22]. Moreover, doping of YBCO samples with another suitable compounds with a right proportion is a reliable method in order to achieve highly qualified complex structures [23] with

improved grain boundary superconducting properties [24]. In our previous research we have shown that the  $J_c$  can be significantly enhanced by adding small amount of carbon nanotube (CNTs) indicating the formation of pinning centers in YBCO matrix [25]. Following up the same motivation, the aim of this work is to investigate the impact of carbon nanofibers (CNFs) on the structural and transport properties of YBCO and compared it with those obtained via CNTs addition. Co-precipitation method was used to prepare the samples which we believed that the powders obtained by this technique have good homogeneity and fine grain. The method is a relatively low cost method as it is cheaper over other “solution” methods, such as sol gel, spray drying and freeze drying [26, 27].

## 2 Experimental details

Metal acetate (Yttrium, Barium, and Copper) and oxalic acid (high purity powders  $\geq 99.9\%$  supplied by Alfa Aesar) were weighed in appropriate molar ratios with the required stoichiometric ratios of  $\text{Y}^{3+}$ ,  $\text{Ba}^{2+}$ , and  $\text{Cu}^{3+}$  (1:2:3, respectively). The cations were mixed in solution added with 0.5 M oxalic acid and then dissolved in 2-propanol and distilled water until became precipitate of a mixed oxalate system. As a result, blue precipitate slurry was obtained. The powders were calcined for 36 h at 900 °C. The calcined powders were ground into fine particulates and mixed thoroughly with CNFs (CNFs, Nanostructured & Amorphous Materials “NanoAmor”, Diameter 39–50 nm, length  $> 1 \mu\text{m}$ ) of different weight percentages (0, 0.2, 0.4, 0.6 and 0.8 wt%) before being pressed into pellets. Those concentrations were selected due to their optimal value which is in range with the improvement in their superconducting properties later. The pellets were then sintered at 920 °C for 45 h in air.

Electrical resistance measurements were carried out using standard four-probe method, in a closed cycle helium cryostat at temperature between 25 and 300 K. Silver paint was used as contact points between the four tiny wires and the sample. From the measurement, the value of onset critical temperature ( $T_{c\text{-onset}}$ ) and offset critical temperature ( $T_{c\text{-offset}}$ ) were determined. Transport critical current density ( $J_c$ ) was measured on bar-shaped samples at the temperature of 30 K in self-fields (zero magnetic fields).

Crystal structure and phase formation were identified via X-ray diffraction using Philips 1710 diffractometer with  $\text{CuK}_\alpha$  radiation source. Morphology and grain size were identified by scanning electron microscope for each sample.

### 3 Results and discussion

#### 3.1 Four point probe measurement

Normalized resistance as a function of temperature measurement between 25 and 300 K was carried out on the samples and the transition temperature,  $T_c$  is shown in Fig. 1. The addition of CNFs changed the metallic behavior of normal state in the pure sample to semiconducting behavior in the samples of  $x = 0.2\text{--}0.8$  wt%. The pure  $\text{YBa}_2\text{Cu}_3\text{O}_{7-\delta}$  shows the highest  $T_{c\text{-onset}}$  and  $T_{c\text{-offset}}$  at 90.5 K and 85.5 K, respectively. The  $T_{c\text{-onset}}$  and  $T_{c\text{-offset}}$  were found to decrease with increasing CNFs content from  $x = 0.2$  wt% to  $x = 0.8$  wt%. Among the samples with CNFs addition, sample  $x = 0.4$  wt% gives high  $T_c$  at 88 K and narrow  $\Delta T_c$  ( $T_{c\text{-onset}} - T_{c\text{-offset}}$ ) = 22 K, compared with samples  $x = 2, 6$  and  $8$  wt%. The high  $T_c$  is due to the homogeneity of the sample, improvement of crystallinity, and increment in the grain size [28–30]. The statement is verified by SEM analysis of average grain size calculation. The average grain size is calculated by using ImageJ software and its sizes of grains are all mentioned in Sect. 3.4. The variation of  $\Delta T_c$  as pictured in Fig. 2 shows the broadening of the resistive transition of 0.4 wt% sample is the narrowest compared to other wt% addition of 0.2 and 0.8 with  $\Delta T_c$  of 24 K and 30 K, respectively. The value of broadening is supported with the  $T_c$  value measured. In other words, the broadened resistive transition reduces as a result of the enhancement in the crystallinity and grain connectivity.

#### 3.2 Transport critical current density, $J_c$

Transport  $J_c$  is the maximum current that can flow through a cross-sectional area before a superconductor is restored to normal state. This area is one of the criterions used to determine  $J_c$  besides transport critical current ( $I_c$ ).  $J_c$  can be identified from V to I plots as illustrated in Fig. 3.  $J_c$  was calculated using the equation  $J_c = I_c/A$  [31], where A is cross-sectional area of the bar-shaped sample.  $J_c$  for the pure sample

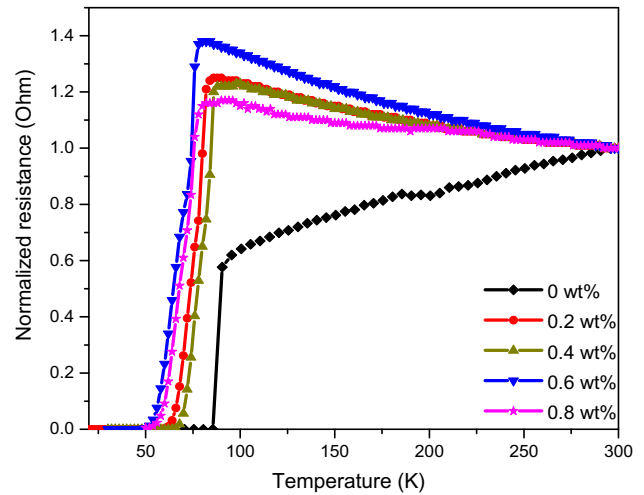


**Fig. 1** Normalized resistance against temperature at different weight percentage of  $x = 0, 0.2, 0.4, 0.6$  and  $0.8$  wt%

at low temperature 30 K and self-field shows a low value of  $11 \text{ A/cm}^2$ . Self-field means when no external magnetic field is applied during the measurement. However, enhancement of  $J_c$  is proved through the influence of the CNFs addition. It is noted that the self-field  $J_c$  increases dramatically to  $830 \text{ A/cm}^2$  with the CNFs addition for sample  $x = 0.4$  wt%. Such enhancement in  $J_c$  could be related to the improved grain connectivity [23, 24]. The variation of the transport  $J_c$  of the pure and samples with CNFs addition is as shown in Fig. 4, where one order enhancement in the  $J_c$  value is observed for samples with  $x = 0.4$  wt% and  $x = 0.6$  wt%. However, when CNFs is increased beyond  $x = 0.6$  wt%,  $J_c$  decreased due to the decrease in  $T_c$ . Thus, the optimum value

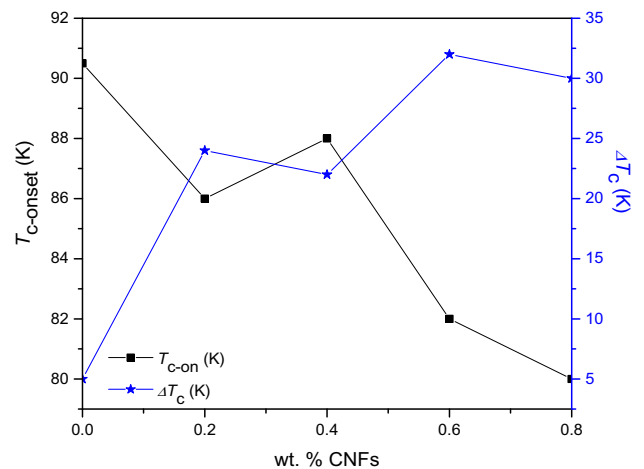


**Fig. 2**  $T_{c\text{-onset}}$  (K) and variation of  $T_c$  at  $x = 0, 0.2, 0.4, 0.6$  and  $0.8$  wt%

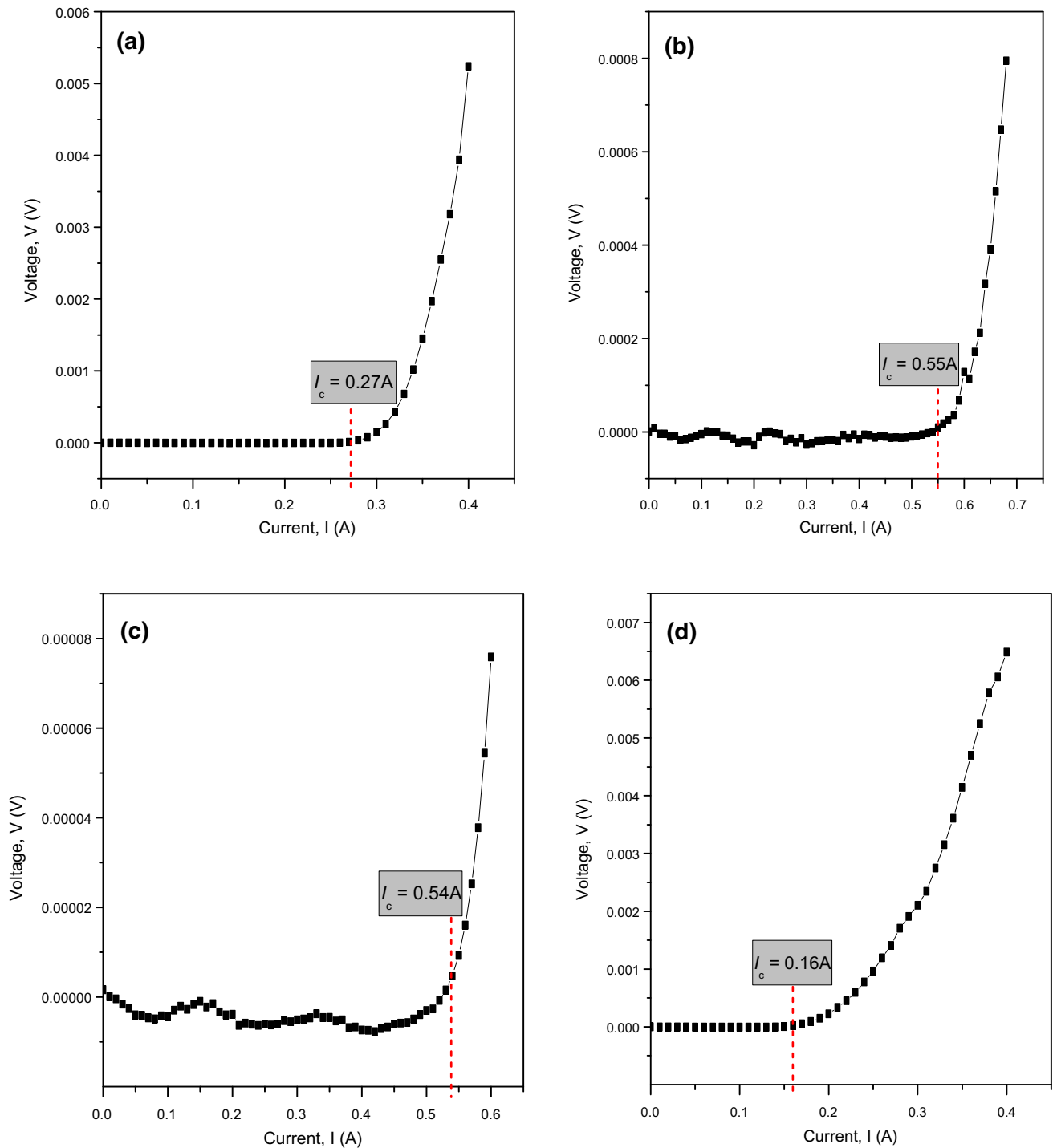


**Fig. 3** V–I curve in self-field at 30 K of **a**  $x = 0.2$  wt% **b**  $x = 0.4$  wt% **c**  $x = 0.6$  wt% **d**  $x = 0.8$  wt%

for impurities concentration was verified with the small percentage. The limited addition of impurities in YBCO superconductors enhances its optimal superconductivity by expanding the superconducting grain size [32] and upgraded the current-carrying capacity of Y-123 [7, 33]. Nevertheless, the value of  $J_c$

decreases above 0.4 wt% of addition, due to the diminishment of  $T_c$  suggesting that CNFs addition destroys the superconducting state [34].

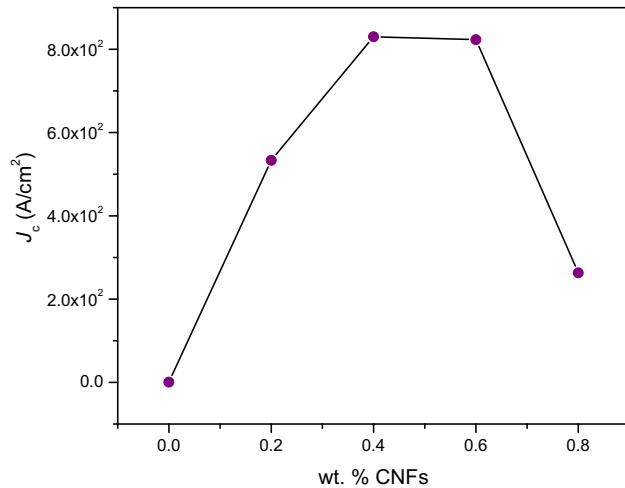


**Fig. 4** The variation of transport  $J_c$  against CNFs content

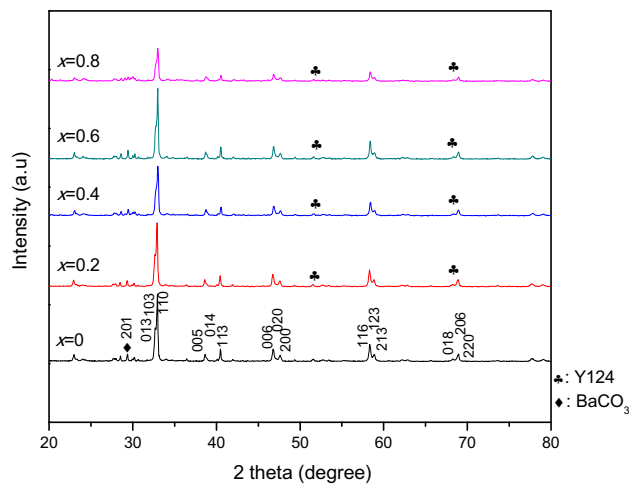


**Fig. 5** XRD spectra of  $\text{YBa}_2\text{Cu}_3\text{O}_{7-\delta}$  with varying CNFs content ( $x = 0, 0.2, 0.4, 0.6,$  and  $0.8$  wt%)

### 3.3 Structural analysis

XRD spectra of all five samples are presented in Fig. 5. The highest intensity diffraction peaks are recorded at approximately  $32.91^\circ$  and  $32.94^\circ$  belonging to the indices of (103) and (110) respectively, for orthorhombic perovskite Y-123 phase. By analyzing the patterns, the orthorhombic structure (Pmmm) space group of Y-123 phase (ICDD file: 98-002-4641) is dominant for all samples with the existence of some impurity peaks. Some of the peaks were indexed to  $\text{YBa}_2\text{Cu}_4\text{O}_8$  or Y-124 (ICDD file: 98-004-0146). The presence of (202) peaks at  $68.24^\circ, 68.59^\circ, 68.49^\circ$  and  $68.46^\circ$  respectively confirmed the formation of Y-124 in the CNFs added samples ( $x = 0.2, 0.4, 0.6$  and  $0.8$  wt%). Reflections of CNFs were not observed in the patterns due to the fact that the amount of CNFs addition ( $x$  values) could be too small. In other words, there is no peak from CNFs as observed in the XRD patterns of the added samples, showing that those they could have diffused into the crystal structure of the bulk Y-123 [24]. The lattice parameter  $c$ -axis decreased with increasing amount of CNFs addition. The percentage of Y-123 phase reduced and the volume of unit cell decreased slightly with the increasing of CNFs concentration. The percentage of Y-124 phase for all added samples is tabulated in Table 1. It is also clear from Table 1 that the formation of  $\text{BaCO}_3$  vanished with CNFs addition. However, the crystallographic structure remains in the orthorhombic form. The orthorhombicity factor which is defined as  $(b - a)/(a + b)$ , where  $a$  and  $b$  are lattice parameters of Y-123, was

**Table 1** Lattice parameter  $a, b, c$ , volume of unit cell, volume fraction of all phases and grain size

$x$ (wt%)	$a$ (Å)	$b$ (Å)	$c$ (Å)	Orthorhombicity factor	Volume of unit cell (Å <sup>3</sup> )	Volume fraction of Y-123 (%)	Volume fraction of Y-124 (%)	Volume fraction of BaCO <sub>3</sub> (%)	Grain size (nm)
0.0	3.8277 ± 0.0003	3.8864 ± 0.0004	11.6813 ± 0.0015	0.0076	173.770	96.2	–	3.8	545 ± 11
0.2	3.8271 ± 0.0002	3.8851 ± 0.0003	11.6783 ± 0.0012	0.0075	173.645	97.6	2.4	–	514 ± 13
0.4	3.8314 ± 0.0004	3.8860 ± 0.0005	11.6781 ± 0.0019	0.0071	173.875	96.3	3.7	–	666 ± 14
0.6	3.8315 ± 0.0004	3.8876 ± 0.0005	11.6775 ± 0.0019	0.0074	173.942	94.5	5.5	–	740 ± 10
0.8	3.8315 ± 0.0005	3.8874 ± 0.0008	11.6752 ± 0.0029	0.0073	173.899	92.7	7.3	–	664 ± 12

**Fig. 6** SEM images of **a** Y-123 + CNFs ( $x = 0.2$  wt%) **b** Y-123 + CNFs ( $x = 0.4$  wt%) **c** Y-123 + CNFs ( $x = 0.6$  wt%) **d** Y-123 + CNFs ( $x = 0.8$  wt%)

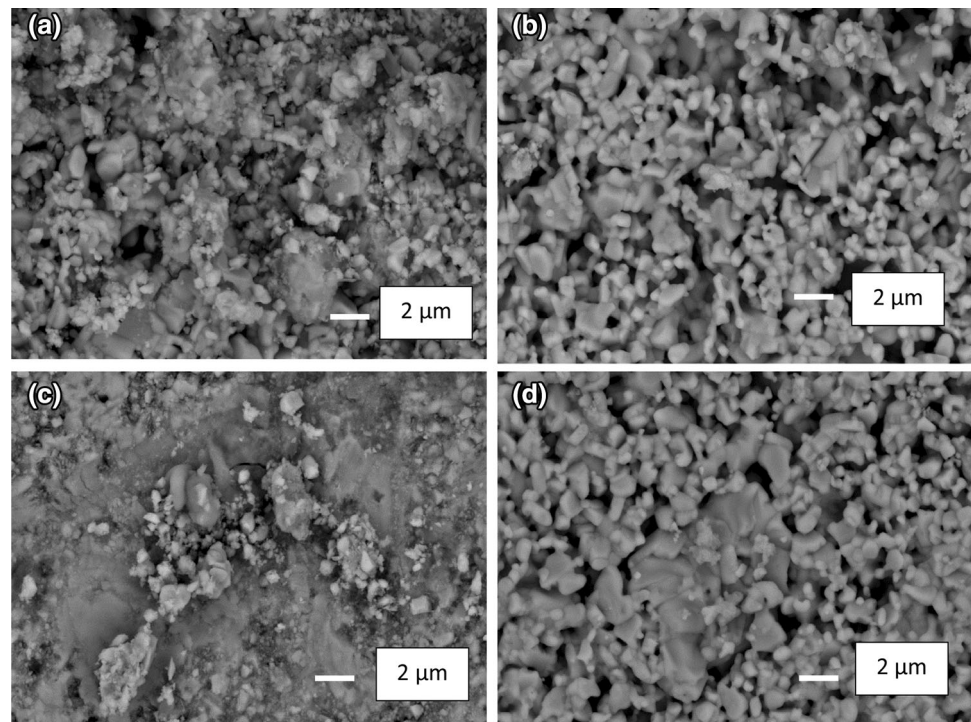


**Fig. 7** EDX analysis of sample  $x = 0.2$  and  $0.8$  wt%

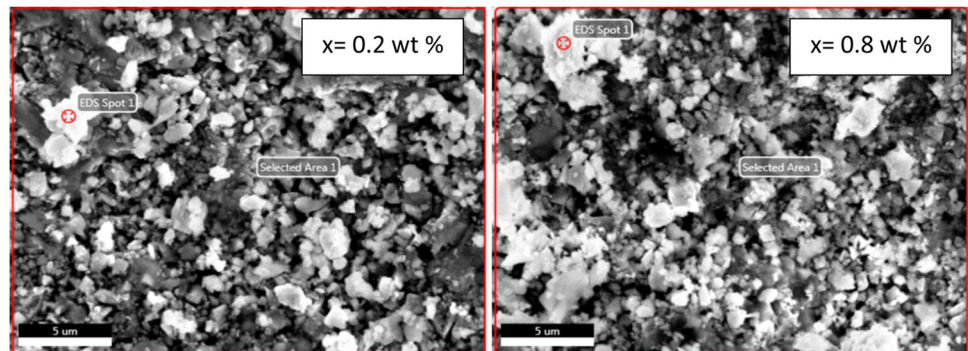


**Table 2** The atomic percentage of C, Y, Ba, Cu element of samples  $x = 0.2$  wt% and  $x = 0.8$  wt% from EDX analysis

Sample	Atomic %			
	C	Y	Ba	Cu
$x = 0.2$ wt%	56.69	7.07	14.61	21.63
$x = 0.8$ wt%	63.96	5.90	12.42	17.72

calculated and shown in Table 1. The orthorhombicity factor decreased with the 0.2–0.8 wt% CNFs addition. The crystallinity of the sample with  $x = 0.2$  wt% CNFs addition improved as indicated by the intensity of XRD peaks and orthorhombicity factor.

### 3.4 Microstructural analysis

To further understand the role of CNFs addition, SEM images of surface morphology for the samples as shown in Fig. 6a–e were investigated. The surface morphology of CNFs added samples (0.2–0.8 wt%) as shown in Fig. 6a–d respectively were closely imaged with resolution of  $10 \mu\text{m}$  and magnification of  $\times 5000$ . As the nanoparticles of carbon source were increasingly added into the pure sample, the grain size seems to increase within the range of 514–740 nm. The average grain size of 0.8 wt% of CNFs addition was measured to be 664 nm. Sample  $x = 0.4$  wt%, (Fig. 6b) shows good homogeneity as well as the increment in the grain size in comparing with sample lower wt% which result in enhanced  $T_c$

and  $J_c$ . This addition level of CNFs might act as columnar defects that were proven to be very strong pinning centers in high temperature superconductor compounds [4].

Figure 7 shows the EDX analysis of the samples  $x = 0.2$  and  $0.8$  wt%. The EDX spots were performed over white regions distributed in Y-123 matrix. Quantitative analysis of the EDX data was summarized in Table 2. The result revealed that those spots were enriched with C element which proved that CNFs were well distributed in the Y-123 samples. The atomic percentage of carbon in the selected spots increased with increasing  $x$  (see Table 2). The elemental composition ratio of the spots being investigated was very close to the nominal composition of  $\text{YBa}_2\text{Cu}_3\text{O}_{7-\delta}$  which is approximately 1:2:3. These results give a probability that the major phase is Y-123. The EDX elemental analysis confirmed the increment of carbon element with CNFs addition although they were not detected from the XRD patterns. This might be due to the too small amount of carbon needed to detect by the latter technique.

## 4 Conclusions

This study shows experimentally that the addition of nanoparticles CNFs can significantly enhance the critical current density,  $J_c$  of bulk  $\text{YBa}_2\text{Cu}_3\text{O}_{7-\delta}$ . The increase of  $J_c$  using suitable impurities as the artificial pinning centers demonstrates a promising route for the enhancement of the flux pinning properties. Thus, the  $x = 0.4$  wt% CNFs added sample shows the optimum amount of addition as it exhibits the highest  $T_c$  and  $J_c$  among the added samples. Furthermore, the sample has the biggest average grain size and highest percentage of Y-123 phase respectively. Finally, all the samples are proved to be shown the major phase of  $\text{YBa}_2\text{Cu}_3\text{O}_{7-\delta}$  as supported by the elemental EDX analysis.

## Acknowledgements

This work was supported by the Ministry of Higher Education, Malaysia (MOHE) under the ERGS (ERGS/1-2013/5527174), and also partly supported by Sakura Science Program (aPBL), Shibaura Institute of Technology (SIT) under the Top Global University

Project, Designed by Ministry of Education, Culture, Sports, Science and Technology in Japan.

**Open Access** This article is licensed under a Creative Commons Attribution 4.0 International License, which permits use, sharing, adaptation, distribution and reproduction in any medium or format, as long as you give appropriate credit to the original author(s) and the source, provide a link to the Creative Commons licence, and indicate if changes were made. The images or other third party material in this article are included in the article's Creative Commons licence, unless indicated otherwise in a credit line to the material. If material is not included in the article's Creative Commons licence and your intended use is not permitted by statutory regulation or exceeds the permitted use, you will need to obtain permission directly from the copyright holder. To view a copy of this licence, visit <http://creativecommons.org/licenses/by/4.0/>.

## References

1. M.K. Wu, J.R. Ashburn, C.J. Torng, P.H. Hor, R.L. Meng, L. Gao, Z.J. Huang, Y.Q. Wang, C.W. Chu, *Phys. Rev. Lett.* **58**, 908–910 (1987)
2. P.H. Hor, L. Gao, R.L. Meng, Z.J. Huang, Y.Q. Wang, K.M. Forster, J. Vassiliou, C.W. Chu, M.K. Wu, J.R. Ashburn, C.J. Torng, *Phys. Rev. Lett.* **58**, 911–912 (1987)
3. R.A. Hawsey, D.K. Christen, *Phys. C* (2006). <https://doi.org/10.1016/j.physc.2006.04.062>
4. S. Dadras, Y. Liu, Y.S. Chai, V. Daadmehr, K.H. Kim, *Phys. C* **469**, 55–59 (2009)
5. S.N. Abd-Ghani, R. Abd-Shukor, K. Wei, *Advanced Materials Research*. (2012). <https://doi.org/10.4028/www.scientific.net/AMR.501.309>
6. S. Gupta, R.S. Yadav, B. Das, *ISST J. Appl. Phys.* **2**, 1–5 (2011)
7. S.B. Guner, O. Gorur, S. Celik, M. Dogruer, G. Yildirim, A. Varilci, C. Terzioglu, *J. Alloys Compd.* **540**, 260–266 (2012)
8. R. Mawassi, S. Marhaba, M. Roumie, R. Awad, M. Korek, I. Hassan, *J. Supercond. Novel Magn.* **27**, 1131–1142 (2014)
9. P. Mikheenko, J.S. Abell, V.S. Dang, M.M.A. Kechik, J.L. Tanner, P. Paturi, H. Huhtinen, N. Hari Babu, D.A. Cardwell, A. Crisan, *J. Phys. Conf. Ser.* **234**, 1–10 (2010)
10. M.M.A. Kechik, *Improvement of Critical Current Density in  $\text{YBa}_2\text{Cu}_3\text{O}_{7-\delta}$  Films with Nano-inclusions* (University of Birmingham, Birmingham, 2010), pp. 21–26
11. A. Sarkar, V.S. Dang, P. Mikheenko, M.M.A. Kechik, J.S. Abell, A. Crisan, *Thin Solid Films* **519**, 876–879 (2010)

12. S.K. Pathak, N.H. Babu, K. Iida, T. Denis, L. Matthews, M. Strasik, D.A. Cardwell, *Mater. Sci. Eng. B* **151**, 40–46 (2008)
13. V.S. Dang, *Nanotechnology of Pinning Centres in High Temperature Superconducting YBa<sub>2</sub>Cu<sub>3</sub>O<sub>7</sub> Films* (University of Birmingham, Birmingham, 2010), p. 29
14. L. Zhou, S.K. Chen, K.G. Wang, X.Z. Wu, P.X. Zhang, Y. Feng, H.H. Wen, S.L. Li, *Phys. C* **371**, 62–68 (2002)
15. A. Hamrita, Y. Slimani, M.K. Ben Salem, E. Hannachi, L. Bessais, F. Ben Azzouz, M. Ben Salem, *Ceram. Int.* **40**, 1461–1470 (2014)
16. R. Abd-Shukor, M.M.A. Kechik, S.A. Halim, *J. Phys.: Conf. Ser.* **97**, 012050 (2008)
17. A. Ramli, A.H. Shaari, H. Baqiah, C.S. Kean, M.M.A. Kechik, *J. Rare Earths* **34**, 895 (2016)
18. S.E. Shirsath, C. Cazorla, T. Lu, L. Zhang, Y. Yan Tay, X. Lou, Y. Liu, S. Li, D. Wang, *Nano Lett.* **20**(2), 1262–1271 (2020)
19. N.N. Mohd Yusuf, M.M.A. Kechik, H. Baqiah, S.K. Chen, K.P. Lim, A.H. Shaari, W.N.W. Wan Jusoh, S.I. Mousa Dihom, Z.A. Talib, R. Abd-Shukor, *Materials* **12**, 92 (2019)
20. A. Ghasemi, S.E. Shirsath, X. Liu, A. Morisako, *J. Appl. Phys.* **109**, 07A507 (2011)
21. A. Ghasemi, S.E. Shirsath, X. Liu, A. Morisako, *J. Appl. Phys.* **111**, 07B543 (2012)
22. N.M. Hapipi, S.K. Chen, A.H. Shaari, M.M.A. Kechik, K.B. Tan, K.P. Lim, *J. Mater. Sci.: Mater. Electron.* **29**, 18684–18692 (2018)
23. M. Tepe, Y. Uzun, U.S. Gokay, *J. Supercond. Novel Magn.* **28**, 541–544 (2015)
24. J.Y. Xiang, C. Fleck, D.P. Hampshire, *J. Phys. Conf. Ser.* **97**, 1–7 (2008)
25. N.A. Khalid, M.M.A. Kechik, N.A. Baharuddin, S.K. Chen, H. Baqiah, N.N.M. Yusuf, A.H. Shaari, A. Hashim, Z.A. Talib, *Ceram. Int.* **44**, 9568–9573 (2018)
26. S.E. Shirsath, D. Wang, S.S. Jadhav, M.L. Mane, S. Li, *Ferrites Obtained by Sol–Gel Method* (Springer International Publishing, Cham, 2018), pp. 695–735
27. E.A. Duarte, N.G. Rudawski, P.A. Quintero, M.W. Meisel, J.C. Nino, *Supercond. Sci. Technol.* **28**(1), 015006 (2015)
28. K. Sato, S. Ohara, *Trans. JWRI* **38**(1), 85–88 (2009)
29. I. Schildermans, M. Van Bael, E. Knaepen, J. Yperman, J. Mullens, L.C. Van Poucke, *Phys. C* **278**, 55–61 (1997)
30. N.J. Azman, H. Abdullah, R. Abd-Shukor, *Adv. Condens. Matter Phys.* (2014). <https://doi.org/10.1155/2014/498747>
31. W. Gao, Z. Li, N.M. Sammes, *Introduction to Electronic Materials for Engineers*, 2nd edn. (World Scientific Publishing Company, Singapore, 2011), p. 309
32. P. Rani, R. Jha, V. Awana, *J. Supercond. Novel Magn* **26**, 2347–2352 (2013)
33. H. Salamati, A.A. Babaei-Brojeny, M. Safa, *Supercond. Sci. Technol.* (2001). <https://doi.org/10.1088/0953-2048/14/10/302>
34. S. Xu, A. Yu, Y. Gu, X. Wu, *J. Rare Earths* **28**, 434–436 (2010)

**Publisher's Note** Springer Nature remains neutral with regard to jurisdictional claims in published maps and institutional affiliations.